International Forum on Aeroelasticity and Structural Dynamics
IFASD 2017
25-28 June 2017 Como, Italy

WIND TUNNEL EVALUATION OF A STATIC OUTPUT FEEDBACK CONTROLLER FOR GUST LOAD ALLEVIATION ON A REGIONAL AIRCRAFT

Federico Fonte[1], **Sergio Ricci**[1], **Paolo Mantegazza**[1]

[1]Department of Aerospace Engineering
Politecnico di Milano
Via La Masa, 34 Milano 20156 Italy
federico.fonte@polimi.it
ricci.sergio.polimi.it
paolo.mantegazza@polimi.it

Keywords: Gust load alleviation, static output feedback, wind tunnel test

Abstract: The paper describes the design of a Static Output Feedback (SOF) controller for gust load alleviation and its evaluation on a wind tunnel model of a regional aircraft. The design of the controller is based on the numerical minimization of the $\mathcal{H}_2$ norm of the closed loop system. The optimization is performed using a state-space description of the flexible aircraft which includes also the dynamics of the actuation system and of the sensors. The controller has been evaluated experimentally on a half-span wind tunnel model, in the experimental campaign the robustness of the controller has been evaluated by varying the flight condition.

1 INTRODUCTION

The interest toward active load control system is continuously growing thanks to the improvement of digital control systems and of tools available for the design and evaluation of such systems. Among the various efforts performed in design and analysis of active load alleviation systems, the clean sky GLAMOUR project aims at the experimental evaluation of such systems using a wind tunnel half-span flexible model [1].

This work describes the design of a Static Output Feedback (SOF) controller aimed at the reduction of gust loads in the wing structure. The controller was designed on a linear model of the aircraft and eventually tested on a wind tunnel aeroelastic model with actuated control surfaces (inner and outer aileron, elevator) and free to move in pitch and plunge. It represents an half-span model of a regional transport aircraft and it has been built under the Clean Sky GLAMOUR project. A gust generator installed in the large wind tunnel of Politecnico di Milano provides the excitation while responses are obtained at different flight speeds and with different excitations.

2 AIRCRAFT MODEL

The aeroelastic analyses and the design of the control system were performed on a numerical model composed by a stick model for the representation of the structure, as shown in Fig. 1(a). The structural properties of the beam elements composing the structure were firstly defined from the scaling of the properties of the reference aircraft, and were continuously updated during the

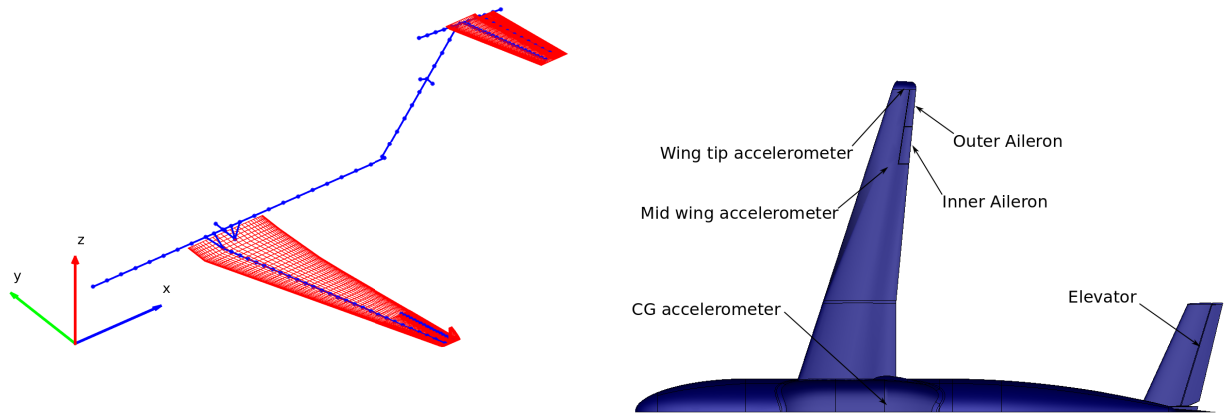

(a) Structural and aerodynamic model (b) Control surfaces and measurement output

Figure 1: Numerical model and input-output definition

design of the model using a detailed finite element model of the aircraft structure. The model is composed by an aeroelastically scaled wing with very stiff fuseage and tail, the rigid movements of plunge and pitch are free thus allowing the complete symmetric response of the aircraft. For the computation of the unsteady aerodynamic forces the Doublet Lattice Method (DLM) was used [2], leading to a frequency domain representation of the aerodynamic transfer function. Since the design of the control system is performed in time domain it was necessary to convert the aerodynamic transfer function in time domain, and this operation was performed using the matrix fraction description approach described in [3].

2.1 Measurement definition

The measurements selected for the design of the control system are the accelerations of three structural points in the wing and center of gravity of the aircraft, considering the component along the vertical motion of the aircraft. The location of the points where accelerations are measured is shown in Fig. 1(b). In addition to the accelerations also the pitch rotation and rotation rate are measured and used by the load alleviation controller. The state-space aeroelastic model of the aircraft is augmented by including the anti-aliasing filters applied to all measurements. From the measured accelerations, velocities and displacements are extracted by means of a pseudo-integrator system, following an approach used in [4], the pseudo-integrator filter has the form

$$y = \frac{s}{s^2 + 2\xi\omega_0 s + \omega_0^2} u \tag{1}$$

where ω_0 defines a cutoff frequency used to remove the static response from the integration, with the double purpose of limiting the action of the controller in steady flight conditions and to remove the drifts that can be associated with a time integration. In this application a value $\omega_0 = 0.4\pi$ was selected.

2.2 Control surface actuation

The model is equipped with three control surfaces: an aileron split in the inboard and outboard sections and the elevator each driven by an electric motor. Since the wing is very thin in correspondence of the ailerons it was not possible to connect directly the motors to the hinge of the control surface, but they were installed in a more forward position chord-wise and connected to the hinge with a pulley-belt mechanism. A dual loop PI/PID controller was then designed with

the purpose of compensating the flexibility of the belt, and at the same time to reproduce the behavior of the actuators of the reference aircraft [5,6]. In order to reproduce the behavior of the actuators of the full-size reference aircraft it was necessary to impose the bandwidth of the control system, along with a saturation in deflection and a torque-dependent saturation in deflection rate. In order to apply these saturations a dual loop structure of the servo system was defined, as shown in Fig. 2. The inner loop performs a feedback on the rotation rate of the motor, and it is driven by a saturated velocity command computed by the outer loop, which operates on the angular position of the control surface. The saturation in deflection is imposed on reference signal of the outer loop, while an observer is used for the estimation of the total torque acting on the control surface hinge, and then for the computation of the rate saturation limits. In order to obtain the linear system used for the optimization of the control system a linearized model of the servo system was obtained, by removing the saturations and using continuous functions for the time derivation of the signals.

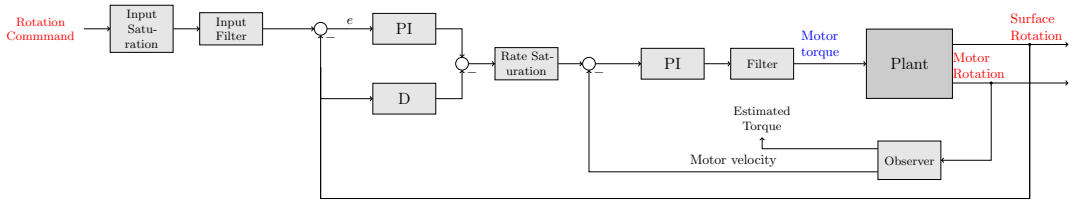

Figure 2: Scheme of the servo controller for the actuation of the control surfaces

3 STATIC OUTPUT FEEDBACK CONTROLLER

The control system is designed as a Static Output Feedback controller, where the control input $\mathbf{u} \in \mathbb{R}^{m_u}$ is obtained from the measurements $\mathbf{y} \in \mathbb{R}^{l_y}$ through a $m_u \times l_y$ gain matrix $\mathbf{G}$ as $\mathbf{u} = \mathbf{G}\mathbf{y}$. The gain matrix is obtained through the minimization of a weighted $\mathcal{H}_2$ norm of the closed loop transfer function, which can be expressed as:

$$J = \int_0^\infty \left[\mathbf{z}^T \mathbf{W}_{zz} \mathbf{z} + \mathbf{u}^T \mathbf{W}_{uu} \mathbf{u}\right] dt \tag{2}$$

where $\mathbf{z}$ represents a set of system outputs whose magnitude need to be reduced, while $\mathbf{W}_{zz}$ and $\mathbf{W}_{uu}$ are weighting matrices, he minimization is obtained through the numerical procedure described in [4].

The performance vector $\boldsymbol{z}$ is composed by the wing root bending and torsional moments, and by the plunge motion of the aircraft, included in order to enforce some damping to its vertical rigid motion, the weights matrices are defined as

$$\boldsymbol{W}_{zz} = \begin{bmatrix} 1 & 0 & 0 \\ 0 & 0.1 & 0 \\ 0 & 0 & 1 \end{bmatrix} \qquad \boldsymbol{W}_{uu} = 7 \times 10^7 \begin{bmatrix} 0.005 & 0 & 0 \\ 0 & 0.005 & 0 \\ 0 & 0 & 1 \end{bmatrix} \tag{3}$$

The disturbance input used for the definition of the closed loop transfer function is the gust input, and a shape filter is used in order to give to the gust input the same frequency content of a deterministic 1-cos gust with frequency $f_g = 0.68 f_{bend}$, where f_{bend} is the frequency of the first wing bending mode of the model. In order to assess the robustness of the controlled system, the gain and phase margins for the simultaneous breaking of all input loops were evaluated [7] obtaining a value of ± 6.2 dB for the gain margin and $\pm 37.8^\circ$ for the phase margin.

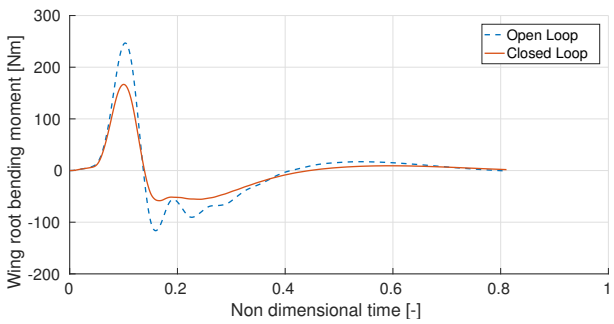

(a) Wing root bending moment

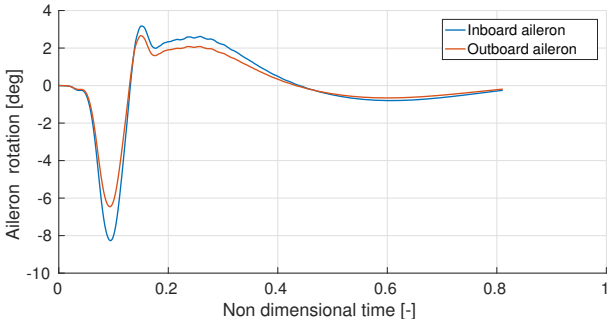

(b) Aileron deflection

Figure 3: Results of linear simulations on the non-correlated model

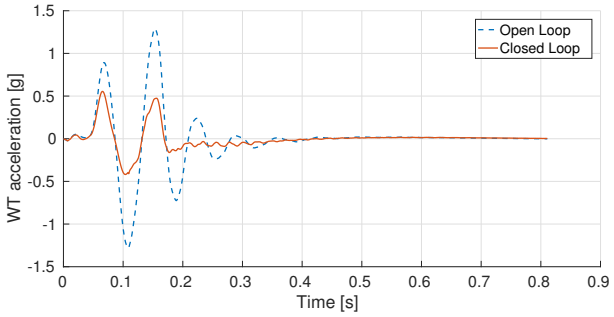

(a) Wing tip acceleration

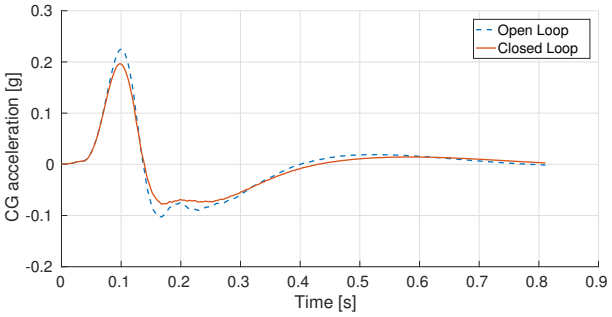

(b) Center of gravity acceleration

Figure 4: Results of linear simulations on the non-correlated model

The results obtained using the linear model are presented in Fig. 3 and Fig. 4, for a gust with frequency $f_g = 0.68 f_{bend}$, and a flight speed equal to V_c, the cruise speed of the aircraft. From Fig. 3(a) it can be seen that the controller is able to reduce the wing root bending moment by 32.5%, reducing its value from 246.8 Nm to 166.7 Nm, with a maximum aileron deflection of about $8°$. In Fig. 4 the accelerations at wing tip and at the center of mass are displayed, showing a large reduction of the wing tip acceleration in the closed loop system, and almost no change in the acceleration of the center of gravity. This is due to the fact that the controller is acting mainly on the ailerons in order to control the wing deformation, while the rigid motion of the aircraft is almost unaffected by the controller, and the elevator deflection is small, lower than $1°$ during all the response.

The Simulink scheme of the final controller is shown in Fig. 5, it can be seen that the three input accelerations are expanded and derived using three pseudo-integrators system, then the deflection command is computed by multiplying the extended input vector by the gain matrix. The controller is implemented in discrete-time with a rate of 100 Hz.

4 WIND TUNNEL MODEL

The SOF controller was applied to the wind tunnel model built within the GLAMOUR project. The model was designed to be installed in the large wind tunnel of Politecnico di Milano, as a testbed for the evaluation of active gust load alleviation techniques. The model represents a regional transport aircraft with an aeroelastically scaled wing and rigid fuselage and tail, and it is free to move in its symmetry plane with pitch and plunge motions.

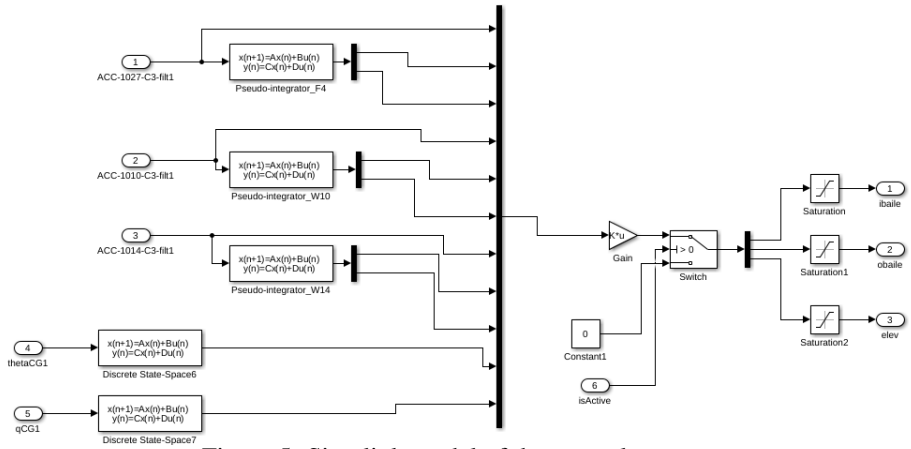

Figure 5: Simulink model of the control system

(a) Actuation system for the vanes (b) Gust generator installed in the wind tunnel

Figure 6: Gust generator device.

4.1 Gust Generator

In order to generate the gust disturbance a gust generator device was designed [8], sizing it in order to generate the gust amplitude required by the regulations [9]. The gust generator is composed by a series of vanes placed on the inlet section of the test chamber, as shown in Fig. 6(b). The gust is generated by rotating them around their quarter chord line by means of a linear electric motor, as shown in Fig. 6(a). A dedicated test campaign was performed in order to map the gust amplitude in the wind tunnel and to verify the ability of the device to produce the desired gust intensity.

4.2 Aeroelastic model

The model is placed horizontally, with its symmetry plane parallel to the floor of the wind tunnel, since the model is free to move in pitch and the dynamic response test are performed around a trimmed flight condition, it is necessary to apply a force to the model able to reproduce the weight force. This is done with the use of a Weight Augmentation System (WAS) composed by a linear electric motor with a force feedback used to apply to the model a constant force, as shown in Fig. 7. A load cell located between the actuator and the model is used for the feedback loop, and a PID controller is used for keeping a reference value for the force.

As said before the model is equipped with a split aileron, and an elevator driven by electric motors. The aileron installation is shown in Fig. 9(a), showing the position of the motors with

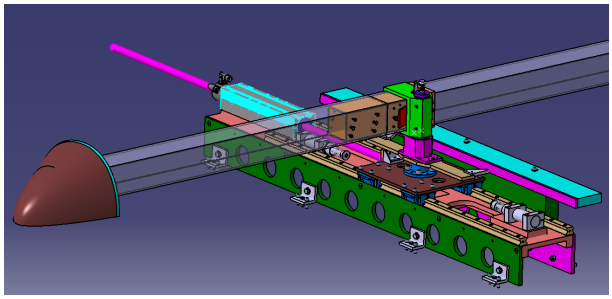

(a) CAD model of the Weight Augmentation System (WAS)

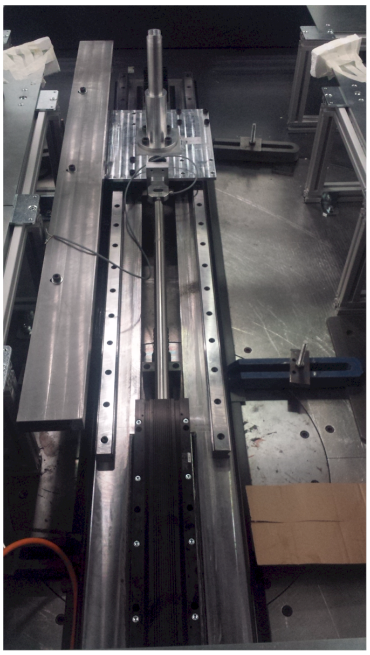

(b) Weight augmentation system installed

Figure 7: Weight augmentation system.

respect to the ailerons, the belts used for the transfer of the motion from the motor to the ailerons and the potentiometers used by the dual loop controller.

The only part of the model aeroelastically scaled is the wing, and it is composed by a carbon fiber spar covered with 3D-printed aerodynamic sectors, as shown in Figures 8(a) and 8(b).

Several Ground Vibration Test (GVT) were performed on the components of the model in order to correlate the numerical model and to check the correspondence between the properties of the model and those of the reference aircraft. Figure 8(c) shows the complete model during the final GVT tests.

4.3 Instrumentation

The model is equipped with a series of sensors, used for the analysis of the response and by the load alleviation controllers. A series of accelerometers is placed along the structure and used both for the GVT tests and the monitoring of the dynamic response, Fig. 9(b) shows the position of the accelerometers on the wing, which are placed in order to provide accelerations in ten stations span-wise, with some double measurement used for the recovery of the torsional motion of the wing. In addition to the accelerometric measurements the rigid pitch and plunge motions of the model are measured by means of a linear and rotational potentiometer, and a gyroscope is used to acquire the pitch rate.

Inside the wing spar ten strain-based measurement stations for the recovery of the loads in the wing. Each station is equipped with a set of strain gauges used in order to recover the bending and torsional moment along the spar. A series of static loading tests were performed in order to calibrate the strain bridges and to obtain the sensitivity between the internal moment and the sensor output, Fig. 9(d) presents the calibration curve for the wing root measurement station, showing the good linearity of the force-strain relation end the low sensitivity to torsional loads.

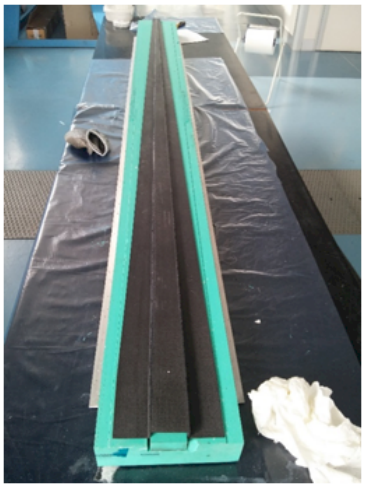

(a) Carbon fiber wing spar

(b) 3D-printed aerodynamic sector.

(c) Complete Model during a GVT test.

Figure 8: Wind tunnel model

5 RESULTS

The dynamic response tests are performed at different wind tunnel speed and with different gust frequencies. The two flight speeds correspond to the cruise speed for the aircraft V_c and to the dive speed $V_d = 1.2V_c$, an additional robustness test has been performed at a flight speed of $V_r = 1.46V_c$. The generated gust has a time profile similar to a 1-cos shape, for each flight speed two different frequencies of the gust shape were tested, that is a frequency equal to that of the first wing bending mode of the aircraft f_{bend}, and a lower frequency, equal to $0.68 f_{bend}$ which corresponded to the most critical load condition for the reference aircraft.

5.1 Updated numerical model

On the basis of the results of the open loop dynamic responses it was possible to correct the numerical model with respect to the model used for the design of the control system, in particular

- The results of the GVT on the complete model and on the tail components were used to tune the elastic properties of the fuselage and the tail.
- Some damping in pitch and plunge needed to be added in order to reproduce the effect of the friction.
- A correction factor had to be applied to reduce the aerodynamic moments generated by the surface deflection, with respect to the values prescribed by the DLM.

The numerical aeroelastic model is then augmented with the nonlinear servo system, introduced by including in the Simulink model the same C code used for the actual real-time implementation of the controller obtained using the RTAI interface [10]. Finally the input gust to the system is no more the analytic 1-cos gust but it is the one obtained from the experimental data taken during the characterization of the gust generator device. Figure 9 presents the time history of the pitch rate during a positive gust load condition. It can be seen how the experimental data presents an higher amplitude of the response. The same increase in amplitude can be seen also

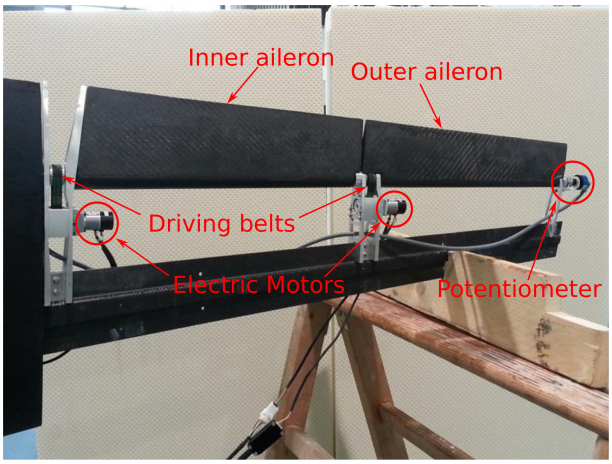

(a) Control system for the aileron actuation

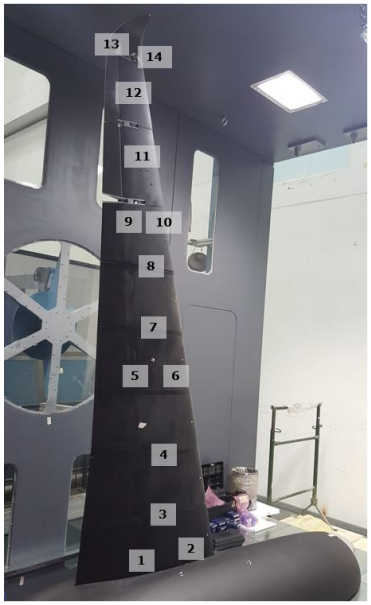

(b) Position of the accelerometers in the wing

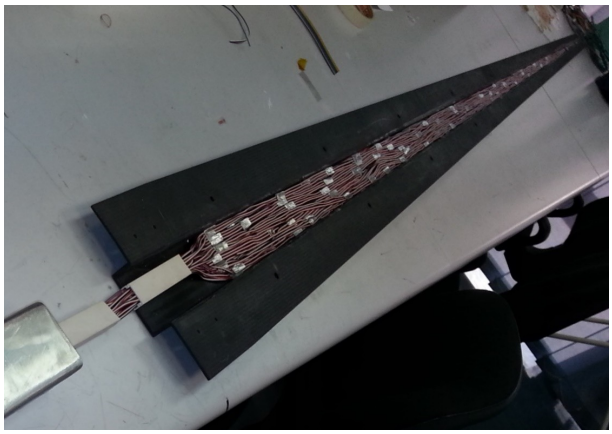

(c) Strain gauges installation in the wing spar

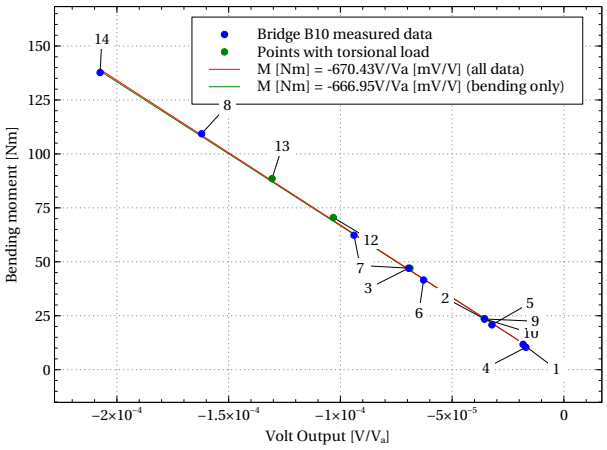

(d) Calibration curve for the strain bridges

in the other measured quantities like loads and accelerations and suggests an increase of the amplitude of the gust load with respect to the value used in the numerical model. In the results shown here, however no such increment was added.

5.2 Experimental results

The experimental results confirm the ability of the system to reduce the dynamic loads acting on the wing. As an example of the responses obtained, Figures Fig. 10, Fig. 11, Fig. 12 and Fig. 13 show the time histories of the wing root bending moment, the aileron deflection and the wing tip and center of gravity accelerations for four different load conditions associated with a positive gust.

The aileron deflection required by the control system and the actual deflection of the surface are compared in Fig. 10(b), Fig. 11(b), Fig. 12(b) and Fig. 13(b), the difference is due to the dynamics of the servo system which imposes a limited bandwidth to the aileron deflection

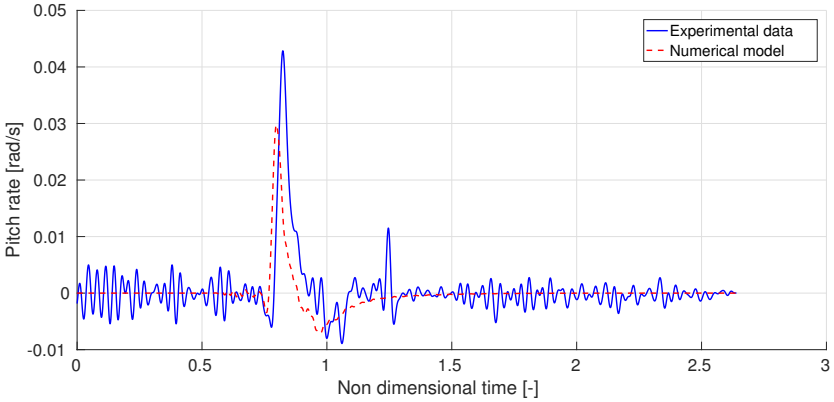

Figure 9: Pitch rate for $V = V_c$, $f_g = f_{bend}$

V/V_c	f_g/f_{bend}	sign	OL	CL	reduction
1	0.68	+	238.49	205.31	13.91%
1	0.68	−	252.34	223.13	11.57%
1	1.00	+	209.56	192.74	8.03%
1	1.00	−	211.34	191.41	9.43%
1.2	0.68	+	195.08	168.19	13.78%
1.2	0.68	−	185.80	143.15	22.95%
1.2	1.00	+	175.68	151.32	13.86%
1.2	1.00	−	175.28	157.19	10.32%
1.46	0.68	+	227.60	227.26	0.16%
1.46	0.68	−	206.48	172.25	16.57%

Table 1: Results from sensitivity analysis

along with rate saturations. The commanded deflection never reaches the saturation limit, set to $15°$, but is able to activate the saturation limit as can be seen by the almost linear increment in Fig. 12(b). It can also be noticed how the saturation limit helps improving the correlation between the numerical model and the experimental data, since it leads to the same surface deflection out of two different deflection commands.

The accelerometric measurements were affected by a high level of noise, compared to the signal amplitude, especially for the acceleration of the center of mass, which resulted to be of lower amplitude with respect to the one predicted by the linear numerical model. This effect led to the oscillations in the second part of the response that can be seen in Fig. 12(c), and that are not present in the response of the numerical model. The accelerations shown in Figures from 10(b) to 13(b) are filtered with a lowpass filter with cutout frequency 10 Hz.

It can be noticed how in general the controller is able to reduce the maximum load in a consistent way, as it can also be seen in Tab. 1 where a summary of the results obtained is presented and it can be noticed that the reduction is of the order of 10% in all the configurations analyzed.

The results obtained shows that a slight increase in the dynamic pressure leads to a better performance for the controller, but the gain disappear at higher velocities, as said before this can be partially due to the presence of high measurement noise in the acceleometric channels, but it also comes from the different behavior of the model in this flight condition with respect to that in the cruise speed condition that has been used for the design of the controller.

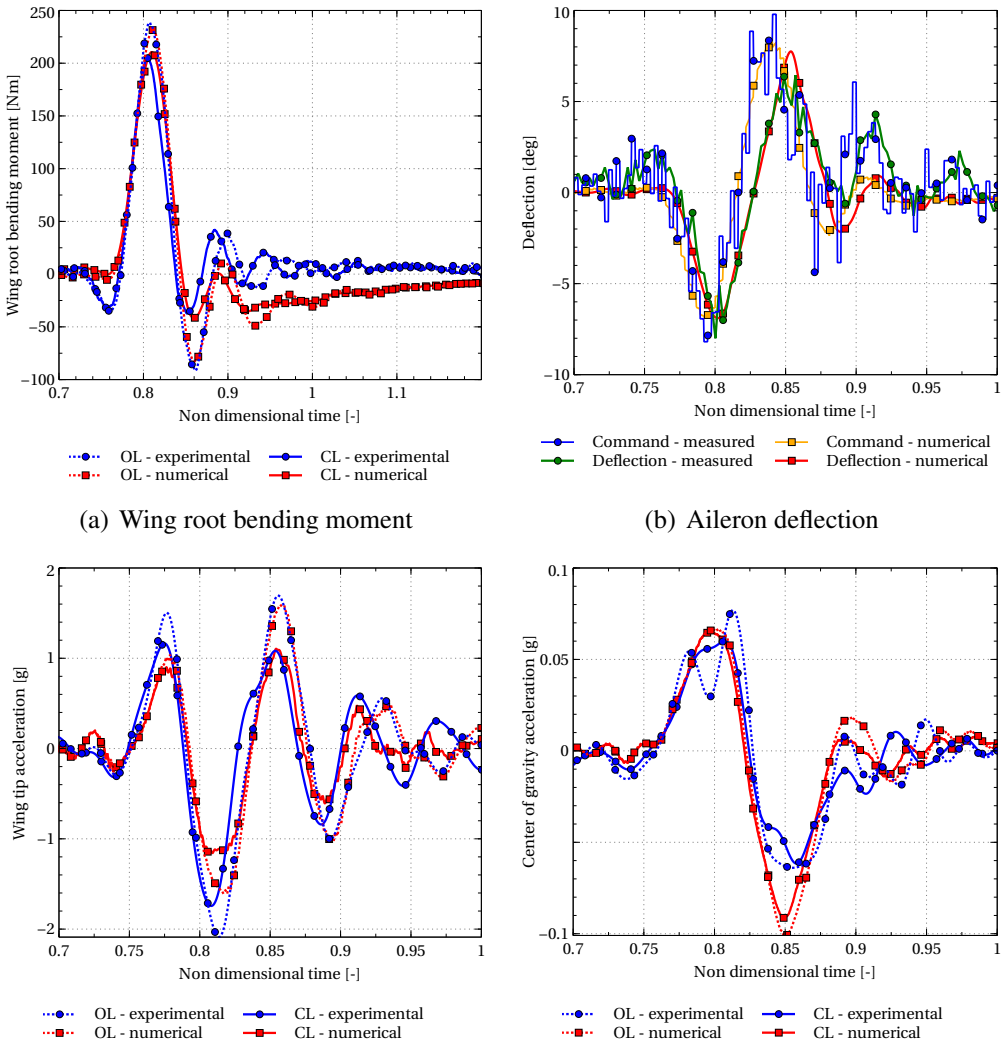

(a) Wing root bending moment

(b) Aileron deflection

(c) Wing tip acceleration

(d) Center of gravity acceleration

Figure 10: Results for positive gust, $V = V_c$, $f_g = 0.68 f_{bend}$

6 CONCLUSIONS

The results presented in this work demonstrate the capability of a gust load alleviation controller. The system proved to provide consistent performances even in spite of differences between the model used for the design of the controller and the actual conditions for its use, partly given to different structural properties and also given by the need to apply the same controller to different flight conditions without a rescheduling. The results obtained here can be of interest in actual implementations since they shows how robust can be a control implementation based on a static controller and accelerometric measurements, with a system able to reduce structural load after being designed on a low-fidelity model that can then be tuned after experimental data are available.

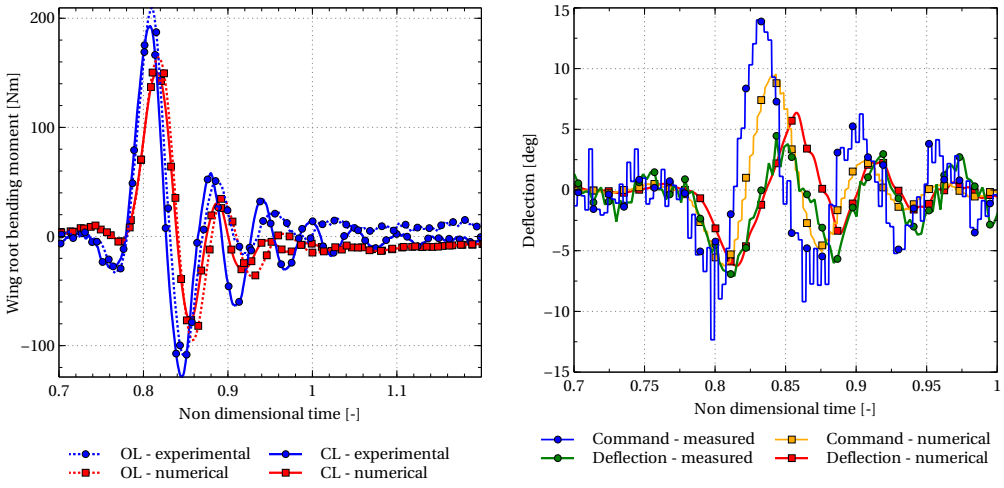

(a) Wing root bending moment

(b) Aileron deflection

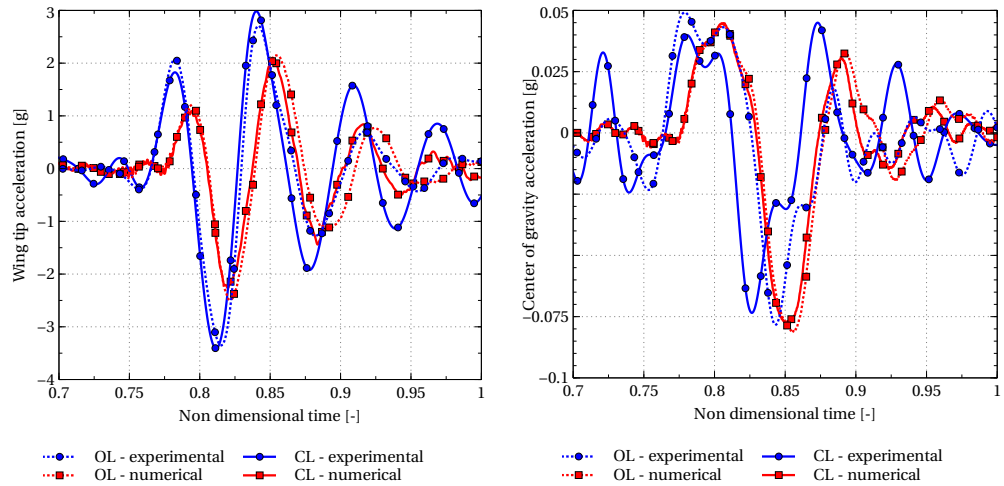

(c) Wing tip acceleration

(d) Center of gravity acceleration

Figure 11: Results for positive gust, $V = V_c$, $f_g = f_{bend}$

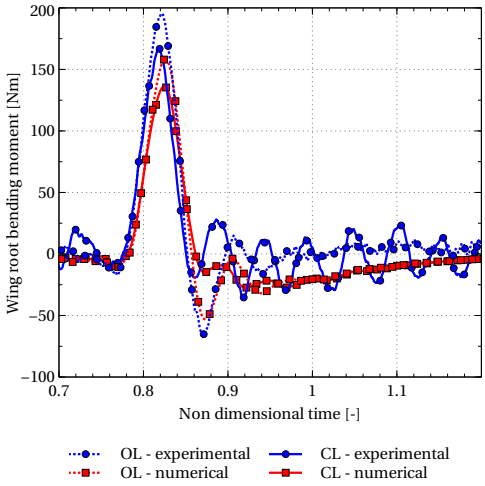

(a) Wing root bending moment

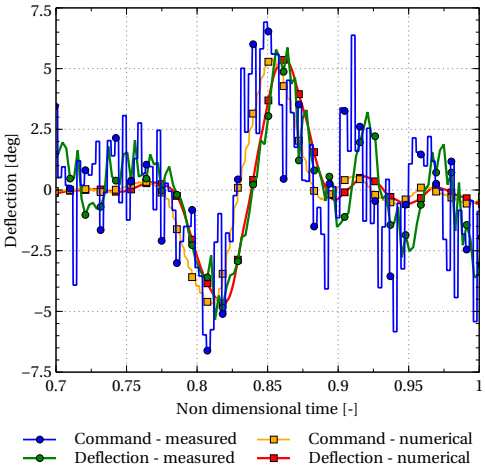

(b) Aileron deflection

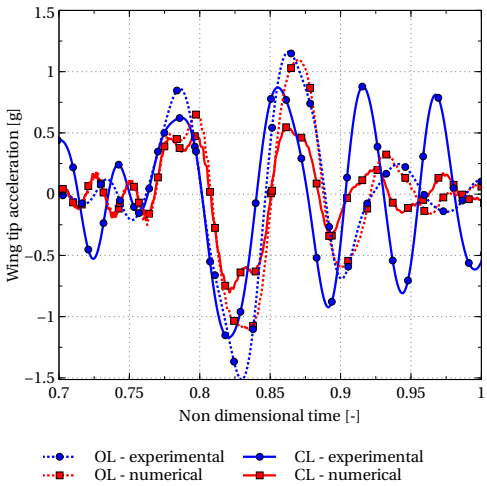

(c) Wing tip acceleration

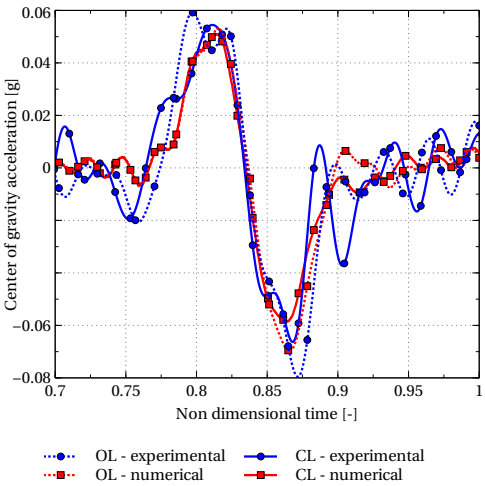

(d) Center of gravity acceleration

Figure 12: Results for positive gust, $V = 1.2V_c$, $f_g = 0.68f_{bend}$

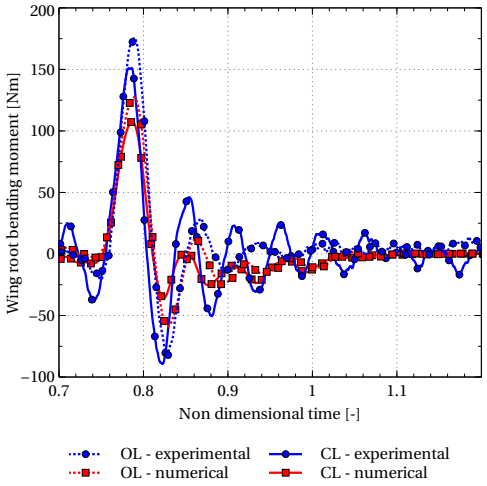

(a) Wing root bending moment

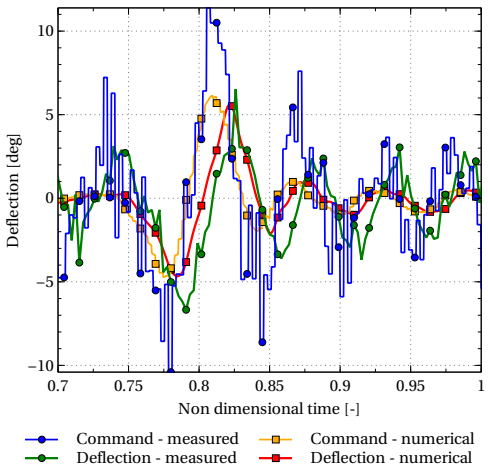

(b) Aileron deflection

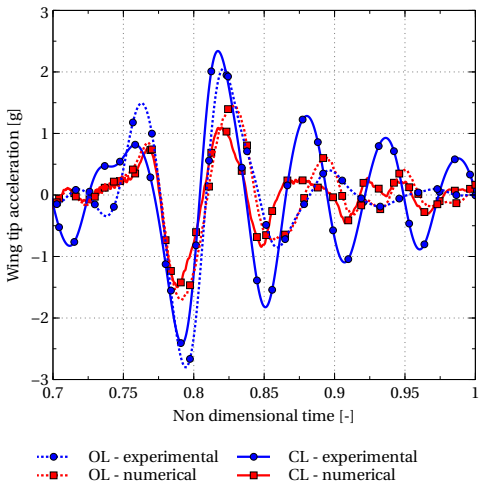

(c) Wing tip acceleration

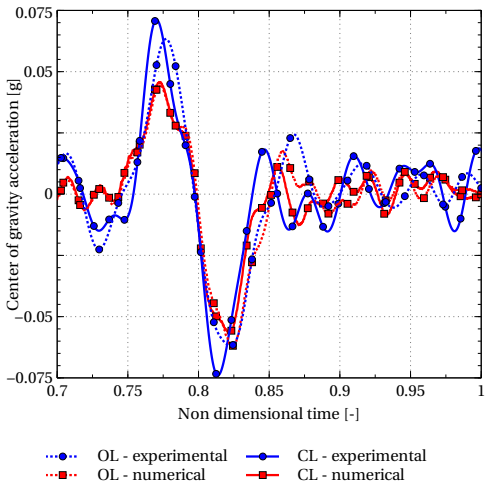

(d) Center of gravity acceleration

Figure 13: Results for positive gust, $V = 1.2V_c$, $f_g = f_{bend}$

7 ACKNOWLEDGEMENTS

The research leading to these results has received funding from the European Community's Seventh Framework Programme (FP7/2007-2013) for the Clean Sky Joint Technology Initiative under Grant Agreement for Partners no. 620084. A special thanks is due to Alessandro De Gaspari, Luca Riccobene, Francesco Toffol and Edoardo Vigoni who made most of the work required for the design and construction of the wind tunnel model.

8 REFERENCES

[1] Ricci, S., De Gaspari, A., Riccobene, L., et al. (2017). Design and wind tunnel test validation of gust load alleviation systems. In *58th AIAA/ASCE/AHS/ASC Structures, Structural Dynamics, and Materials Conference*. p. 1818.

[2] Albano, E. and Rodden, W. P. (1969). Doublet-lattice method for calculating lift distribution on oscillating surfaces in subsonic flow. *AIAA Journal*, 7(2), 279–285.

[3] Ripepi, M. and Mantegazza, P. (2013). Improved Matrix Fraction Approximation of Aerodynamic Transfer Matrices. *AIAA Journal*, 51(5), 1156–1173. doi:10.2514/1.J052009.

[4] Fonte, F., Ricci, S., and Mantegazza, P. (2015). Gust load alleviation for a regional aircraft through a static output feedback. *Journal of Aircraft*, 52(5), 1559–1574.

[5] De Gaspari, A., Mannarino, A., and Mantegazza, P. (2016). Design and realization of the control surfaces actuation system within the glamour project. *Aerotecnica Missili & Spazio*, 95(4).

[6] De Gaspari, A., Mannarino, A., and Mantegazza, P. (2017). A dual loop strategy for the design of a control surface actuation system with nonlinear limitations. *Mechanical Systems and Signal Processing*, 90, 334–349.

[7] Blight, J. D., Dailey, R. L., and Gangsaas, D. (1994). Practical control law design for aircraft using multivariable techniques. *International Journal of Control*, 59(1), 93–137. doi:10.1080/00207179408923071.

[8] Fonte, F., Riccobene, L., Ricci, S., et al. (2016). Design, manufacturing and validation of a gust generator for wind tunnel test of a large scale aeroelastic model. In *30th Congress of the International Council of the Aeronautical Sciences*.

[9] AAVV (2009). Certification Specifications for Large Aeroplanes CS-25. amendment 7 ed., European Aviation Safety Agency. Annex to ED Decision 2009/013/R.

[10] Beal, D., Bianchi, E., Dozio, L., et al. (2000). Rtai: Real-time application interface. *Linux Journal*, 29(10).

COPYRIGHT STATEMENT